PAPER

Check for updates

Tailoring the efficiency of porphyrin molecular frameworks for the electroactivation of molecular N2†

María Romero-Angel, [ID] ‡[a] Roumayssa Amrine,‡[b] Beatriz Ávila-Bolívar,[b] Neyvis Almora-Barrios, [ID] [a] Carolina R. Ganivet,[a] Natalia M. Padial, [ID] [a] Vicente Montiel, [ID] [b] José Solla-Gullón, [ID] *[b] Sergio Tatay [ID] *[a] and Carlos Martí-Gastaldo [ID] *[a]

The combination of compositional versatility and topological diversity for the integration of electroactive species into high-porosity molecular architectures is perhaps one of the main appeals of metal–organic frameworks (MOFs) in the field of electrocatalysis. This premise has attracted much interest in recent years, and the results generated have also revealed one of the main limitations of molecular materials in this context: low stability under electrocatalytic conditions. Using zirconium MOFs as a starting point, in this work, we use this stability as a variable to discriminate between the most suitable electrocatalytic reaction and specific topologies within this family. Our results revealed that the PCN-224 family is particularly suitable for the electroreduction of molecular nitrogen for the formation of ammonia with faradaic efficiencies above 30% in the presence of Ni^{2+} sites, an activity that improves most of the catalysts described. We also introduce the fluorination of porphyrin at the *meso* position as a good alternative to improve both the activity and stability of this material under electrocatalytic conditions.

Introduction

The structural and compositional versatility intrinsic to metal–organic frameworks (MOFs) and their ultrahigh porosity make them interesting platforms for catalysis. Compared to metal complexes, metal oxides, and zeolites, to name a few, the molecular nature of MOFs enables an exquisite level of control over their structural, chemical, and physical properties. Their large internal surface areas and high density of active sites can facilitate substrate accessibility and mass transport for better catalytic performance.[1] Also, the isolation of catalytic sites in the framework backbone can contribute to the stabilization of highly reactive intermediates whereas the ordered arrangement of molecular components can help delineate structure–activity relationships to support the design of improved catalysts. Besides, for a given geometry and connectivity of the linker and metal node, MOFs can exist in different topologies, that will result in different pore sizes, dimensionalities (*i.e.* mass transport), coordination geometries and variable densities of the

active sites.[2–5] On top of this, the pore environment around the active site can be further modified to regulate redox properties and binding energies of the metal centers, stabilize intermediates, promote proton transfer, or locally modify proton concentration.[6]

Provided the samples have sufficient chemical stability, their use in photo and electrocatalytic processes is of great importance to demonstrate the potential of reticular design in catalysis.[7] MOFs have been used as catalysts with promising results in reactions as the hydrogen evolution reaction (HER),[8] oxygen reduction/evolution reaction (ORR/OER),[9] CO$_2$ reduction reaction (CO$_2$RR),[10] and nitrogen reduction reaction (NRR).[11] Porphyrin molecules are particularly appealing in this context. Besides their intrinsic electrocatalytic activity in solution,[12–14] their rigid and robust backbones allow for the assembly of reticular frameworks with fine control over their intermolecular distance, their density, the chemical environment, and greater/lower accessibility to substrates depending on the net porosity of the material. This ease to direct framework assembly is supported by the huge number of porphyrin-MOFs reported with different metal nodes and secondary building units (SBUs).[15–17] Among them, Zr/carboxylate-based SBUs, in particular, those based on the Zr$_6$O$_4$(OH)$_4$ cluster (Zr$_6$), seem to be one of the most synthesized, at least in terms of electrocatalytic efficiency, with at least one member of this subfamily standing out in the HER, OER, CO$_2$RR or NRR. This is arguably due to the superior thermal and water/moisture stability of Zr-MOFs,[18,19]

[a]Instituto de Ciencia Molecular, Universidad de València, c/Catedrático José Beltrán, 2, 46980, Paterna, Spain. E-mail: sergio.tatay@uv.es; carlos.marti@uv.es

[b]Institute of Electrochemistry, University of Alicante, Apdo. 99, E-03080 Alicante, Spain. E-mail: jose.solla@ua.es

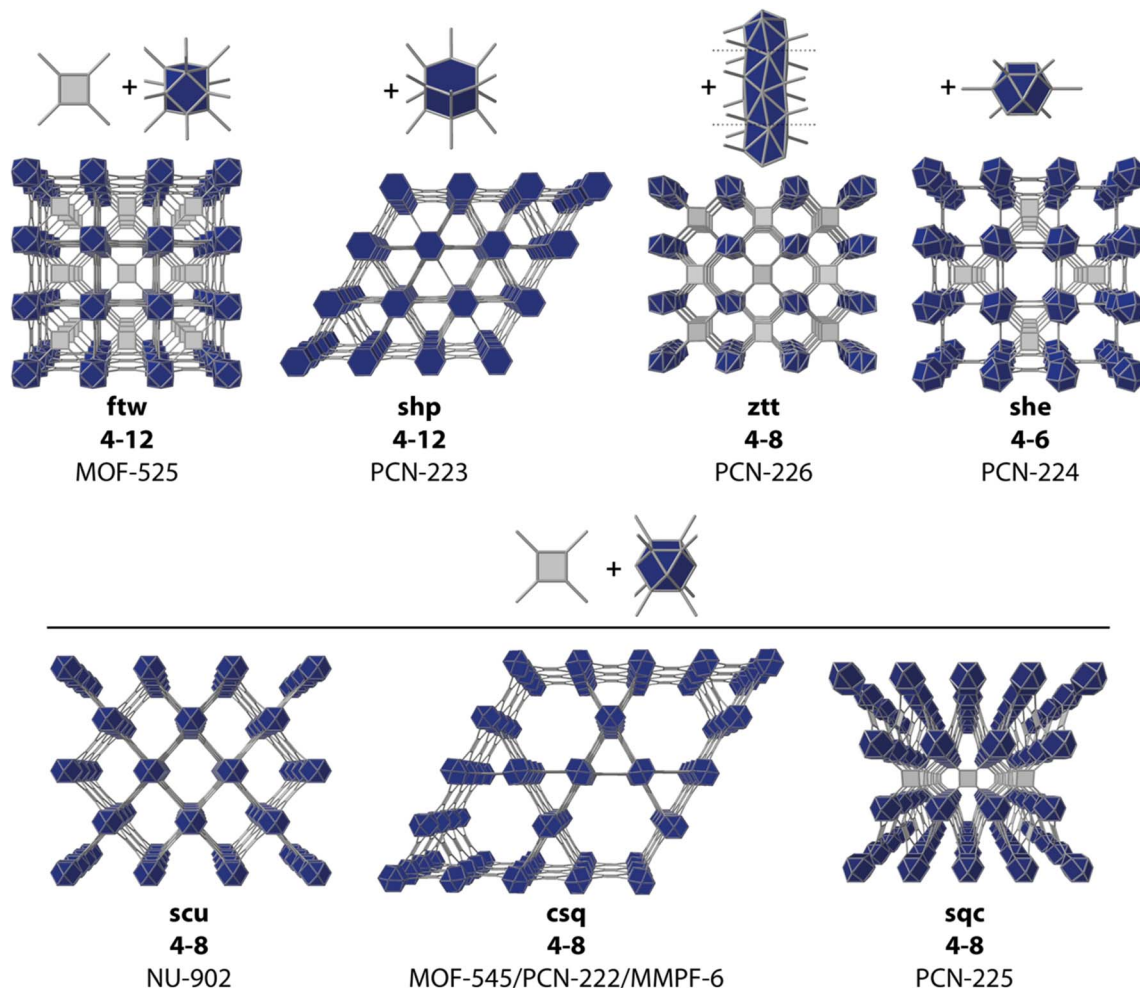‡ These authors contributed to the work equally.

Fig. 1 Some reported topologies for common Zr-oxo clusters and TCPP organic linkers. Representative MOF examples are given for each corresponding net connectivity and topology.

that are expected to prevent their degradation under the conditions imposed by electrocatalytic reactions. The Zr_6 SBU also combines a high versatility in its connectivity index, from 12 to 6 connection points, with a high persistence in dissolution, thus facilitating the synthesis of different topologies with variable porosities for a large pool of potential catalysts (Fig. 1).

Most porphyrin-based molecular frameworks have been built from tetratopic *meso*-tetra(carboxyphenyl)porphyrin (TCPP) linkers, or some other related porphyrins with reduced/increased topicity and/or extended backbones.[20,21] Here we use several representative TCPP–MOFs to systematically study the electrocatalytic activity of such frameworks for ammonia generation as a function of their chemical stability, metal substitution (MTCPP), or the functionalization of the porphyrin ring in the metal position with fluorine atoms (TCPP–F) for tailorable pore environments.

Results and discussion

Framework selection and synthesis

As mentioned above, there are multiple Zr–TCPP MOFs reported, many of which are built from the ubiquitous Zr_6 cluster. However,

this rich variability also imposes some difficulties in controlling their synthesis as phase-pure frameworks due to the formation of defective phases,[22] the concurrent formation of different polymorphs[23] or, different degrees of sensitivity to experimental conditions between different crystallographic phases.[24]

In the search for a synthetically robust platform compatible with the iterative variation of metals and linkers, we chose to test in our laboratory some of the most representative members of the Zr–TCPP MOF family (Fig. 1) including: MOF-525,[24] PCN-223,[25] MOF-545[24] (also referred to as PCN-222[26] and MMPF-6[27]), PCN-224,[28] and PCN-226.[29] The reader should note that in this list we included not only the classical Zr_6 clusters, but also the closely related Zr_8 node and the rod-shape Zr-oxo SBU in PCN-226 for the shake of completeness. We attempted the synthesis of all these MOFs based on the original reported procedures,[24–26,29] except for the case of PCN-224, for which we chose to follow the revisited synthetic protocol recently reported by Lotsch's group.[22] According to our powder X-ray diffraction (PXRD) data (Fig. 2), we straightforwardly obtained phase pure crystalline phases of MOF-525, PCN-224 and PCN-226, while our attempts for the synthesis of MOF-545 and PCN-223 were unsuccessful and yielded amorphous phases. These results
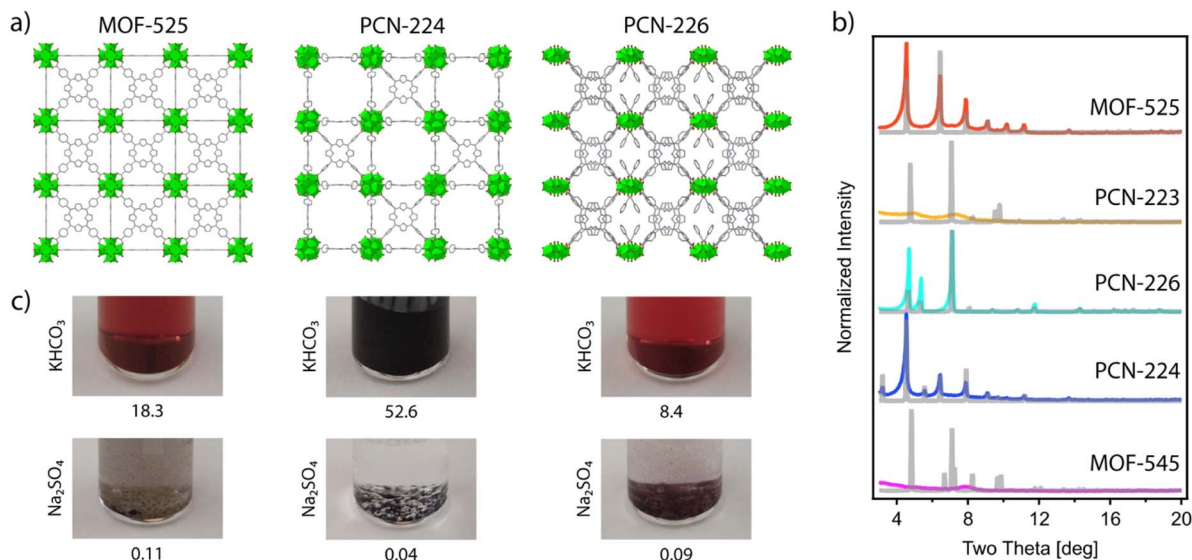
This journal is © The Royal Society of Chemistry 2024

J. Mater. Chem. A, 2024, 12, 10956–10964 | **10957**

Fig. 2 (a) From left to right, crystal structures of the frameworks: MOF-525, PCN-224 and PCN-226. (b) Experimental (colored lines) and simulated (gray lines) PXRD patterns for different Zr–TCCP MOFs referred to in the text. (c) Images showing suspensions of MOF-525, PCN-224, and PCN-226 after immersion at room temperature in KHCO$_3$ and Na$_2$SO$_4$ solutions for 24 h. The numbers below each image show the percentage of Zr leached into the corresponding solution, as determined by ICP.

highlight the difficulty in controlling the synthesis of Zr–TCPP MOF, where different members of the family share very similar or even equal compositions. Our results are in line with recent studies that demonstrate the acute influence of water content on controlling phase formation in Zr–porphyrin-based MOFs[30] and the problems for their synthesis reproducibility due to their sensitivity to slight changes in the experimental conditions.[23,31,32]

As a result of our initial screening, we selected MOF-525, PCN-224, whose crystal structure is represented in Fig. 2c, and PCN-226 as potential platforms to implement our *meta*-substituted TCPP roadmap.

Stability under electrochemical conditions

Among possible applications of Zr–TCPP MOF in electrocatalysis, first we focused on the CO$_2$RR, not only because of the need to find alternatives that contribute to the mitigation of the climate crisis,[33] but also because, in the past decade, porphyrins have attracted remarkable interest for the electrochemical reduction of CO$_2$.[34] These experiments are usually carried out in the presence of basic bicarbonate buffer. Although, Zr-MOFs are often considered relatively stable in alkali media,[18] the presence of bicarbonate makes these reaction conditions somewhat more demanding.[35] In order to examine the chemical stability of the synthesized MOF-525, PCN-224, and PCN-226 frameworks in CO$_2$RR media, the samples were immersed in 0.5 M KHCO$_3$ aqueous solutions at room temperature. After 24 h, solutions had turned dark brown in all cases, and inductively coupled plasma (ICP) analysis confirmed the presence of significant amounts of Zr in the solution that oscillated between 52.6 and 18.3% of the total metal content in the frameworks. This is indicative of a severe degradation associated with the decomposition of Zr-oxo

clusters in this medium, which would be a serious concern for their implementation under electrocatalytic conditions (Fig. 2c). We reasoned that the problem was the coordinating ability of bicarbonate and decided to try some other related catalytic reaction conditions that imposed a less coordinating medium. The key role of ammonia today is as the basic feedstock for inorganic fertilizers that currently support food production for around half of the world's population. Industrial ammonia production is currently derived from fossil fuels and is responsible for the emission of more CO$_2$ than any other chemical-making reaction. Lately, ammonia is also being considered as a renewable energy carrier. For these reasons, the use of the NRR as a sustainable approach to NH$_3$ production is currently being intensely investigated. Compared to other energy related applications, MOFs have been much less studied in this context.[36,37] To confirm the stability of these frameworks under the conditions required for NRR electrochemical tests, we soaked the as-made materials in 0.1 M Na$_2$SO$_4$ aqueous solutions at room temperature. Compared to the use of bicarbonate, all the solutions remained transparent after 24 hours with negligible metal leaching determined by ICP, which remained below 0.11 Zr% in all cases (Fig. 2c).

Our chemical stability tests in conventional aqueous electrolytic solutions suggest that MOF-525, PCN-226 and PCN-224 do not display sufficient chemical stability to be used for the electrochemical CO$_2$RR but they show comparatively higher stability in the medium used for the NRR. Among them, PCN-224 showed the highest chemical stability, displaying a minimum percentage of metal leaching after 24 hours (0.04%). Consequently, PCN-224 is the ideal candidate to investigate the electrochemical activity of the pristine framework or other derivatives belonging to the same family towards the production of ammonia from nitrogen.

PCN-224–M series for electrochemical nitrogen reduction

The nature of the metal centre on the MTCPP unit has been reported to have a marked effect on the catalytic performance.[38–40] Consequently, we synthesized a series of metalated analogues of PCN-224 that we refer to as PCN-224–M (M = Co^{2+}, Ni^{2+}, Cu^{2+}), by reacting $ZrOCl_2$ in the presence of the metalated TCPP porphyrin linkers under the same conditions used for the synthesis of PCN-224. See ESI S2† for the experimental details. According to their PXRD profiles (Fig. 3a), the
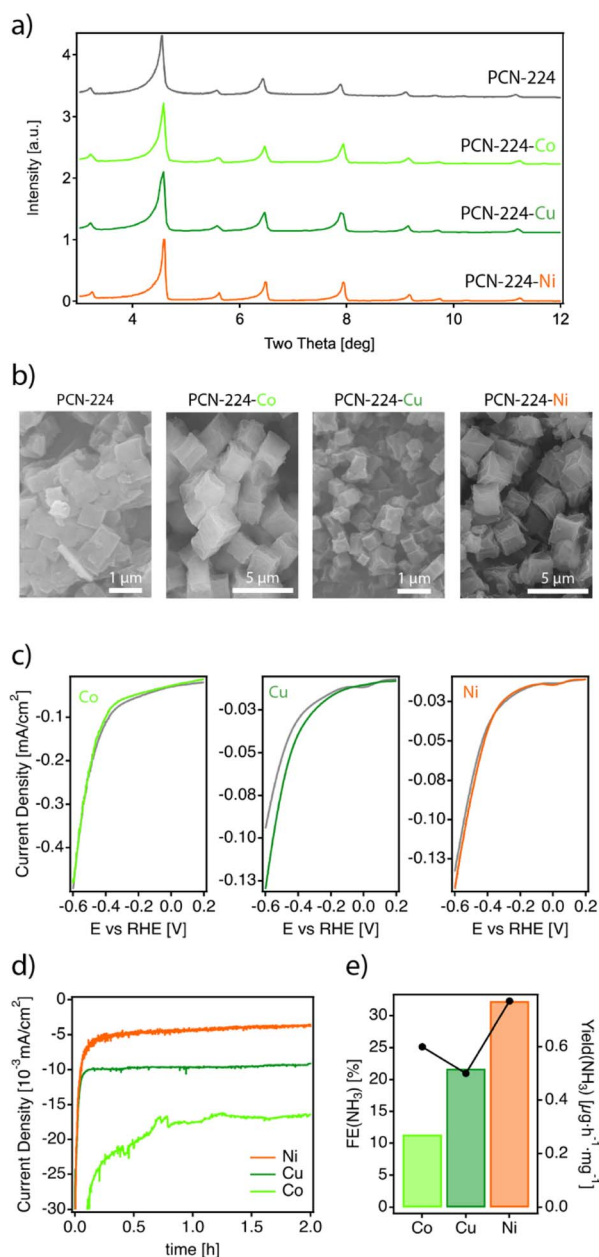

Fig. 3 (a) Powder diffraction of PCN-224 and the metalated PCN-224–M derivatives. (b) SEM images of the isolated solids showing the formation of cube-like crystals with varying sizes. (c) CV at 50 mV s^{-1} for each PCN-224–M framework under an Ar (gray) and N_2 atmosphere (color). (d) CA at −0.04 V vs. RHE for the same materials and (e) comparison of faradaic efficiencies and yields for ammonia generation.

PCN-224–M samples isolated are isostructural to the non-metalated framework confirming the formation of phase pure solids. It is worth noting that we also attempted the synthesis of the PCN-224–Fe analogue. Iron is essential for the biological fixation of molecular nitrogen, and Fe-based compounds have been widely applied industrially in this context.[41] Unfortunately, all our attempts led to the formation of either amorphous solids or the PCN-222–Fe framework (Fig. S10†).[26] Energy dispersive X-ray spectroscopy (EDX) single-point mapping measurements of the PCN-224–M solids confirmed values close to the expected 1 : 4 M/Zr ratio consistent with the corresponding unit formula. Crystal size and morphology were studied by using scanning electron microscopy (SEM). Fig. 3b shows little variation in morphology across the series. All solids display cube-like crystals; however, two different size ranges are observed depending on the sample. While PCN-224–Cu shows crystals of about 1 μm very similar to those of PCN-224, the Co and Ni analogues are comparatively bigger. Leaving aside this small divergence in size, the properties of the PCN-224–M series agree well with the characteristics reported for this MOF and rule out the formation of contaminant oxide phases. Permanent porosity was also analysed with N_2 isotherms at 77 K (Fig. S12†).[28] All samples exhibit a reversible type-I isotherm. While PCN-224 shows the maximum N_2 uptake with a value consistent with that originally reported,[15] the metalated analogues display comparatively lower uptakes as previously reported by others.[42,43]

Next, the electrocatalytic activity of the materials toward the NRR was systematically investigated. For this purpose, electrodes of the different samples were prepared, by mixing the corresponding solids with the binder agent, and sprayed over a Toray carbon paper using an air brushing technique for a final electrode loading of about 0.7 mg cm^{-2}. A platinum wire and a leakless AgCl/Ag (saturated KCl) were used as the counter and reference electrodes, respectively. All potentials were referred to the reversible hydrogen electrode (RHE). Cyclic voltammetry (CV) curves were recorded at 50 mV s^{-1} in Ar and N_2 saturated 0.1 M Na_2SO_4 solution. Chronoamperometry (CA) measurements (electrolysis) were subsequently carried out at −0.04 V, −0.14 V and −0.34 V vs. RHE for 2 h. The experimental details are included in ESI Sections S2 and S7†. It is worth highlighting that these experiments were performed in the same Na_2SO_4 aqueous electrolyte for which we confirmed the stability of PCN-224 under open circuit potential conditions with negligible metal leaching after 24 hours. Faradaic efficiencies (FEs) and ammonia yields were determined using the amount of ammonia produced as determined by the indophenol blue method.[42] Before each electrolysis, five voltammetry cycles between 0.56 V and −0.94 V vs. RHE were recorded to verify the status of the electrodes. Fig. 3c displays the voltammetric profiles corresponding to PCN-224–Co, PCN-224–Ni and PCN-224–Cu in the potential range from 0.2 V to −0.6 V vs. RHE. The voltammetric responses of the electrodes in Ar (gray line) and N_2 (color line) are very similar, with a slight increase of the negative currents in the N_2 saturated solution electrolyte which could be related to an enhanced activity for the electrochemical reduction of N_2 to ammonia. To better evaluate the electrocatalytic properties of the samples towards N_2 electroreduction, CAs were

This journal is © The Royal Society of Chemistry 2024

J. Mater. Chem. A, 2024, **12**, 10956–10964 | **10959**

performed at different potentials of interest. Fig. 3d shows the variation of current density *versus* time at a constant potential of −0.04 V (the potential at which ammonia production reached its maximum) for all catalysts. The results demonstrate that the behaviour of the samples is strongly determined by the type of metal incorporated. In agreement with the voltametric curves (Fig. 3c), Ni and Cu samples exhibited lower current density compared to Co. In addition, all samples showed a relatively stable current during the electrolysis time. Regarding the FE (Table S3†), the results indicate that the FE towards ammonia ranges from 4 to 32% depending on the nature of the metal. Interestingly, in all cases, the highest FE value is achieved at −0.04 V; the Co, Ni, and Cu samples show FE values of about 11.4, 32.3 and 21.7%, respectively. In all cases, the FEs systematically decrease at more negative potentials due to the increased effect of the HER. Thus, at −0.34 V *vs.* RHE, the FE values are the lowest independent of the nature of the electrode. The FE values discussed previously clearly indicate that at a relatively positive potential value of −0.04 V *vs.* RHE, the incorporation of a metal into the PCN-224 framework significantly enhances the electrocatalytic activity of the electrocatalyst, with the Ni metalated being the most efficient one with an FE of about 32%. To rule out the possible contribution of the Toray paper, control experiments were performed with the bare Toray paper electrode. The results are shown in Fig. S27 and S28.† The results indicate the absence of detectable ammonia during these control experiments. To better understand our finding, Fig. 4 compares this 32% FE value with the FEs reported with other electrocatalysts, measured in a comparable range of potentials of ± 0.2 V and obtained in alkaline electrolyte which is expected to suppress the hydrogen evolution reaction for improved NRR activities (Table S4†). The FE of 32.29% registered for PCN-224–Ni is quite higher than the 16.2% reported for the related 2D microporous MOF Fe–TCPP, built from Zn(II) paddlewheel clusters and the metalated TCPP linker.[44,45] Other electrocatalysts prepared by the calcination/pyrolysis of MOFs to generate the corresponding Bi nanoparticles,[46] CeO_2 nanorods[47] Y-stabilized ZrO_2,[48] Co_3O_4 nanopolyhedra,[49] iron doped nanocarbons,[50] or NiO/Ni microtubes[51] all supported on carbon also display comparatively lower activities below a FE of 13%. Higher activities have been reported for other MOF composites reliant on the use of MXenes as ZIF-67@Ti_3C_2,[51] but they are comparatively lower with

efficiencies near 20%. The activity associated with Zr_6 clusters in defective UiO-66 frameworks has been also shown to be very high for this type of reaction with efficiencies up to 48%.[52] This comparison clearly points out the relevance of our results as it implicates the MOF exclusively as a crystalline support of porphyrin complexes acting as electrocatalytic centers.[51] Despite the excellent results in terms of FE, it is important to mention that the electrodes cannot be reused, and the FE values decrease significantly during their second use. This suggests a possible degradation of the electrodes under electrochemical working conditions, which is not obvious for the Cu and Ni derivatives (Fig. S26a†), but is more evident for the cobalt derivative (Fig. S26b†). In the last case, we observed a strong colouration of the solution that agrees well with the characteristic MTCPP UV-vis signals, which was concomitant with the loss of performance. In addition, ICP analysis of the isolated electrolyte solution after electrocatalytic experiments with PCN-224–Ni confirmed an increase in the nickel concentration in the electrolyte buffer of 29.2 ppb compared to the 0.1 ppb present before the reaction, which might be indicative of framework degradation. These results highlight the need to improve the stability of the samples under electrochemical working conditions.

Enhancement of NRR performance by porphyrin functionalization: PCN-224–Ni(F)

The high activity of PCN-224–Ni for electrochemical nitrogen reduction encouraged us to target further improvements, particularly in terms of stability, based on the functionalization of the porphyrin ring. Inspired by similar modifications on molecular catalysts for the electroreduction of CO_2,[12] we prepared the *meta*-fluorinated analogue of TCPP starting from the commercially available linker. As shown in Fig. 5a TCPP–F was obtained from the corresponding methyl esters after hydrolysis in basic media. *Meta*-substituted TCPP–F methyl esters were synthesized in moderate yields by using Lindsey's reaction between pyrrole and commercially available 3-fluoromethyl 4-formylbenzoate to obtain the corresponding TCPP–F methyl esters. In turn, NiTCPP–F was obtained by reacting $NiCl_2$ in DMF at reflux overnight. The NiTCPP–F linker was then reacted with the zirconium salt to produce the corresponding PCN-224–Ni(F) framework according to the same protocol used for the non-fluorinated family. PCN-224–Ni(F) was isolated as micrometric cubes (Fig. 5b). As summarised in ESI Section S4†, the PXRD pattern is consistent with the formation of an isostructural PCN-224 framework with an experimental surface area of 1.400 m^2 g^{-1}. To the best of our knowledge, this is the first example of this family of frameworks prepared from functionalized porphyrin units.

To evaluate the impact of the electron withdrawing fluorine groups on the electrocatalytic NRR we prepared the corresponding electrodes and tested the system under the same conditions used for the PCN-224–M family. The CV of the sample in Ar and N_2-saturated solution was essentially similar to those shown by PCN-224–Ni in Fig. 3c, although for the PCN-224–Ni(F) sample (Fig. 5c), the voltammetric responses revealed an increase in current in the N_2-saturated electrolyte which could be related to an enhanced activity for the electrochemical
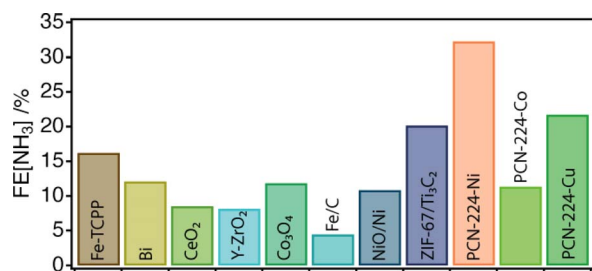

Fig. 4 Overview of the FE of the PCN-224–M family compared to that of other NRR electrocatalysts measured in alkaline electrolytes and under comparable voltage conditions. See ESI Table S1† for more details.
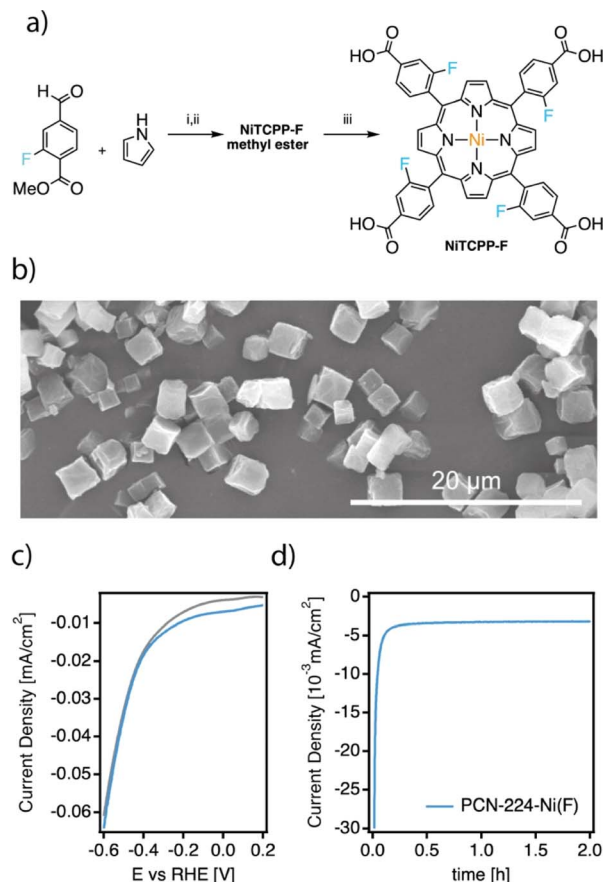
10960 | *J. Mater. Chem. A*, 2024, **12**, 10956–10964

This journal is © The Royal Society of Chemistry 2024

Fig. 5 (a) Experimental procedure for the synthesis of the NiTCCP–F linker: (i) DCM, pyrrole, BF$_3$·OEt$_2$, stirring 2 h, then add p-chloranil, reflux for 2 h, (ii) Ni^{2+}, DMF, reflux overnight, and (iii) MeOH, THF and KOH, reflux overnight and wash with acetic acid. (b) SEM micrograph of PCN-224–Ni(F) crystals. (c) CV at 50 mV s^{-1} under an Ar (gray) and N$_2$ atmosphere (color) and (d) CA at −0.04 V vs. RHE of the fluorinated framework.

reduction of N$_2$ to ammonia. With respect to the FE values (Table S4†), the incorporation of F also improved the FE at −0.04 V, from 32.3% to about 34.5%. As for the unfluorinated samples, for more negative potentials than −0.04 V, the FEs systematically decrease due to the increased effect of the HER.[37] Regarding the ammonia yield rates, a maximum value of 0.9 µg$_{NH_3}$ h^{-1} mg$_{cat}$$^{-1}$ was obtained at −0.04 V vs. RHE. Remarkably, compared to PCN-224–Ni, PCN-224–Ni(F) showed constant FE values up to the third electrode use. This implies an increased stability of the samples under electrochemical working conditions. Hydrophobic fluorination has been used before to enhance MOF stability,[53–55] and in the particular case of the NRR, to increase local concentration of N$_2$ around the catalytic centre, thus limiting proton transportation and favouring the NRR over the HER.[56–58] To confirm the improved stability associated with the incorporation of fluorinated substituents into the porphyrin ring, we analysed the electrolyte solutions after the first electroreduction reaction by ICP. Compared to the near 30 ppb leached by PCN-224–Ni, its fluorinated equivalent is only 4.3 ppb confirming a significant improvement in the stability of this MOF under electrocatalytic

conditions. We also incubated both MOFs in the electrolyte used in the electrocatalytic experiment for 24 h. Fig. S30† shows that while PCN-224–Ni amorphizes considerably under these conditions, the crystallinity of the fluorinated derivative is retained without apparent amorphization. The water isotherms of PCN-224–Ni and PCN-224–Ni(F) at 298 K (Fig. S29†) provide additional evidence of the enhanced stability towards hydrolysis of the fluorinated framework, which is less prone to collapse and displays a much higher water uptake than PCN-224–Ni despite the increase in hydrophobicity.

Although all these experiments support the enhanced stability and reusability of the fluorinated framework, they do not provide a clear answer for the origin of the experimentally observed enhancement of FE. To clarify which was the most likely cause for the observed change in performance, we next carried out DFT calculations.

Computational rationalization of performance

We first performed DFT calculations by using the cluster models representative of the catalytic centers in the corresponding frameworks to obtain the density of states of the MTCPP–X (M = Ni, Co, Cu and X = H, F) units and the adsorption energies of the reactants by using the VASP code and the hybrid functional HSE06. For more details on the computational methodology see ESI Section S9.† Our results only show a small effect of the metal on the electronic structure of the MTCPP units (Table S5 and Fig. S31†), suggesting that the effect of the metal might have a more important role in determining the reaction mechanism in line with previous reports.[59]

Based on these preliminary results we analyzed separately the two generally accepted mechanisms for the NRR. First, we considered an associative Heyrovsky pathway[60] that relies on the adsorption of N$_2$ molecules to the active site followed by hydrogenation, from the combination of protons in solution and electrons from the electrode. However, our simulations reveal that this mechanism is quite unlikely in our case. The binding of N$_2$ with the MTCPP–X units is very weak or metastable with N$_2$–M distances near 3.3 Å in all cases, compared to the 2.0 (Co), 2.5 (Cu), and 2.7 Å (Ni) that would be required for nitrogen adsorption and activation (Fig. S32†).

We next considered the Tafel–Volmer mechanism,[61] which involves hydrogen dissociation (1), electron transfer to the catalyst (2), the adsorption of solvated protons from solution (3), and the adsorption of N$_2$ for its reduction (4). We calculated the adsorption energy for all systems by combining steps (2)–(4) correlating the trends in catalytic activity with the transition metal and fluorination of the porphyrin ring (Fig. 6a). As anticipated by our experimental results, the N$_2$ molecule was preferentially adsorbed in NiTCPP–H and NiTCPP–F, compared to the Co and Cu analogues. According to our calculations, the N$_2$ molecule not only interacts preferably with the Ni site, but also forms a hydrogen bonding with the proton adsorbed by the porphyrin for enhancing adsorption and reducing the energy barrier in the rate determining step (Fig. 6b). This effect is even more acute for a fluorinated framework, for which the electron transfer and nitrogen adsorption are comparatively more
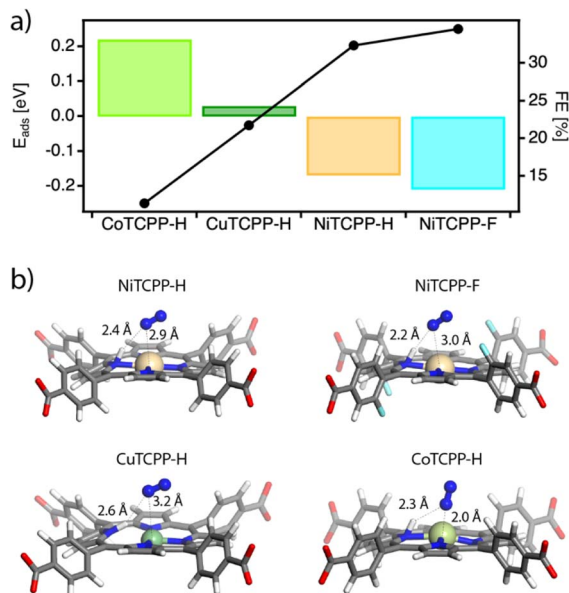
This journal is © The Royal Society of Chemistry 2024

J. Mater. Chem. A, 2024, 12, 10956–10964 | 10961

Fig. 6 (a) DFT adsorption energy (E_{ads}) calculated for MTCPP–X (M = Ni, Co, Cu and X = H, F) cluster models according to the Tafel–Volmer mechanism (left axis) and correlation with the experimental FE values (right axis). (b) Calculated models showing the adsorption of N_2 molecules (in blue) to the catalytic site and distances with the protonated porphyrin in all cases studied.

favourable making it the best electrocatalyst of the family (Table S6†). The addition of the proton to the porphyrin core in CuTCPP–H is stabilized by 0.01 eV, although it elongates the Cu–N interactions with the pyrrole nitrogens by 0.5 Å, suggesting that the N_2 is weakly bound as suggested before by the Heyrovsky mechanism. Finally, the electrons in CoTCPP–H are located at the lowest chemical potentials (2.65 eV) across the series (Table S6†). This suggests a poorer ability for accepting electrons in the first step of the NRR for the lowest electrocatalytic activity of the family.

Conclusions

Based on the topological diversity of Zr MOFs as a starting point, we have identified the PCN-224 family as one of the best candidates for a systematic analysis of their electrocatalytic activity based on their superior chemical stability in the presence of basic aqueous electrolytes. The results obtained in the electroreduction of molecular nitrogen into ammonium reveal a direct impact of the nature of the metal on the electrocatalytic activity, with faradaic efficiency values above 30% for PCN-224–Ni. While this activity is well above that of other reference electrocatalysts in this reaction, our study also reveals important limitations to the reuse of electrodes resulting from a low stability of the MOF under the experimental conditions. The functionalization of porphyrin in the *meso* position has allowed us to synthesize the fluorinated analogue of this framework. PCN-224–Ni(F) displays a significant improvement in the stability of the electrode under equivalent conditions to reach efficiencies close to 35% as a result of its intrinsic hydrophobicity.

Author contributions

All authors contributed to the discussion, participated in the writing of the original draft, and revised the manuscript.

Conflicts of interest

There are no conflicts to declare.

Acknowledgements

Notes and references

1 A. Bavykina, N. Kolobov, I. S. Khan, J. A. Bau, A. Ramirez and J. Gascon, *Chem. Rev.*, 2020, **120**, 8468–8535.

2 M. Li, D. Li, M. O'Keeffe and O. M. Yaghi, *Chem. Rev.*, 2013, **116**, 12466–12535.

3 J. Lyu, X. Zhang, K. Otake, X. Wang, P. Li, Z. Li, Z. Chen, Y. Zhang, M. C. Wasson, Y. Yang, P. Bai, X. Guo, T. Islamoglu and O. K. Farha, *Chem. Sci.*, 2018, **10**, 1186–1192.

4 X. Gong, Y. Shu, Z. Jiang, L. Lu, X. Xu, C. Wang and H. Deng, *Angew. Chem., Int. Ed.*, 2020, **59**, 5326–5331.

5 V. Guillerm and M. Eddaoudi, *Ind. Eng. Chem. Res.*, 2022, **61**, 12641–12648.

6 Z. Ji, H. Wang, S. Canossa, S. Wuttke and O. M. Yaghi, *Adv. Funct. Mater.*, 2020, **30**, 2000238.

7 Y. Peng, S. Sanati, A. Morsali and H. García, *Angew. Chem., Int. Ed.*, 2023, **62**, e202214707.

8 S. Navalón, A. Dhakshinamoorthy, M. Álvaro, B. Ferrer and H. García, *Chem. Rev.*, 2023, **123**, 445–490.

9 (*a*) X. F. Lu, B. Y. Xia, S. Zang and X. W. D. Lou, *Angew. Chem., Int. Ed.*, 2020, **59**, 4634–4650; (*b*) X. Sun, S. Wang, Y. Hou, X. F. Lu, J. Zhang and X. Wang, *J. Mater. Chem. A*, 2023, **11**, 13089–13106.

10 C. Wang, Z. Lv, W. Yang, X. Feng and B. Wang, *Chem. Soc. Rev.*, 2023, **52**, 1382–1427.

11 (*a*) H. Zhong, M. Wang, M. Ghorbani-Asl, J. Zhang, K. H. Ly, Z. Liao, G. Chen, Y. Wei, B. P. Biswal, E. Zschech, I. M. Weidinger, A. V. Krasheninnikov, R. Dong and

10962 | *J. Mater. Chem. A*, 2024, **12**, 10956–10964

This journal is © The Royal Society of Chemistry 2024

X. Feng, *J. Am. Chem. Soc.*, 2021, **143**, 19992–20000; (*b*) Y. Wang, Q. Li, W. Shi and P. Cheng, *Chin. Chem. Lett.*, 2020, **31**, 1768–1772; (*c*) X. Sun, S. Wang, Y. Hou, X. F. Lu, J. Zhang and X. Wang, *J. Mater. Chem. A*, 2023, **11**, 13089–13106.

12 C. Costentin, S. Drouet, M. Robert and J.-M. Savéant, *Science*, 2012, **338**, 90–94.

13 Y. Ishimizu, Z. Ma, M. Hada and H. Fujii, *Inorg. Chem.*, 2021, **60**, 17687–17698.

14 A. Zhang, D. Si, H. Huang, L. Xie, Z. Fang, T. Liu and R. Cao, *Angew. Chem., Int. Ed.*, 2022, **61**, e202203955.

15 W.-Y. Gao, M. Chrzanowski and S. Ma, *Chem. Soc. Rev.*, 2014, **43**, 5841–5866.

16 J. Chen, Y. Zhu and S. Kaskel, *Angew. Chem., Int. Ed.*, 2021, **60**, 5010–5035.

17 Z. Liang, H.-Y. Wang, H. Zheng, W. Zhang and R. Cao, *Chem. Soc. Rev.*, 2021, **50**, 2540–2581.

18 A. J. Howarth, Y. Liu, P. Li, Z. Li, T. C. Wang, J. T. Hupp and O. K. Farha, *Nat. Rev. Mater.*, 2016, **1**, 15018.

19 S. Yuan, L. Feng, K. Wang, J. Pang, M. Bosch, C. Lollar, Y. Sun, J. Qin, X. Yang, P. Zhang, Q. Wang, L. Zou, Y. Zhang, L. Zhang, Y. Fang, J. Li and H. Zhou, *Adv. Mater.*, 2018, **30**, e1704303.

20 B. F. Abrahams, B. F. Hoskins, D. M. Michail and R. Robson, *Nature*, 1994, **369**, 727–729.

21 X. Zhang, M. C. Wasson, M. Shayan, E. K. Berdichevsky, J. Ricardo-Noordberg, Z. Singh, E. K. Papazyan, A. J. Castro, P. Marino, Z. Ajoyan, Z. Chen, T. Islamoglu, A. J. Howarth, Y. Liu, M. B. Majewski, M. J. Katz, J. E. Mondloch and O. K. Farha, *Coord. Chem. Rev.*, 2021, **429**, 213615.

22 C. Koschnick, R. Stäglich, T. Scholz, M. W. Terban, A. von Mankowski, G. Savasci, F. Binder, A. Schökel, M. Etter, J. Nuss, R. Siegel, L. S. Germann, C. Ochsenfeld, R. E. Dinnebier, J. Senker and B. V. Lotsch, *Nat. Commun.*, 2021, **12**, 3099.

23 S. M. Shaikh, P. M. Usov, J. Zhu, M. Cai, J. Alatis and A. J. Morris, *Inorg. Chem.*, 2019, **58**, 5145–5153.

24 W. Morris, B. Volosskiy, S. Demir, F. Gándara, P. L. McGrier, H. Furukawa, D. Cascio, J. F. Stoddart and O. M. Yaghi, *Inorg. Chem.*, 2012, **51**, 6443–6445.

25 D. Feng, Z.-Y. Gu, Y.-P. Chen, J. Park, Z. Wei, Y. Sun, M. Bosch, S. Yuan and H.-C. Zhou, *J. Am. Chem. Soc.*, 2014, **136**, 17714–17717.

26 D. Feng, Z.-Y. Gu, J.-R. Li, H.-L. Jiang, Z. Wei and H.-C. Zhou, *Angew. Chem., Int. Ed.*, 2012, **124**, 10453–10456.

27 Y. Chen, T. Hoang and S. Ma, *Inorg. Chem.*, 2008, **51**, 12600–12602.

28 D. Feng, W.-C. Chung, Z. Wei, Z.-Y. Gu, H.-L. Jiang, Y.-P. Chen, D. J. Darensbourg and H.-C. Zhou, *J. Am. Chem. Soc.*, 2013, **135**, 17105–17110.

29 M. O. Cichocka, Z. Liang, D. Feng, S. Back, S. Siahrostami, X. Wang, L. Samperisi, Y. Sun, H. Xu, N. Hedin, H. Zheng, X. Zou, H.-C. Zhou and Z. Huang, *J. Am. Chem. Soc.*, 2020, **142**, 15386–15395.

30 C. Koschnick, M. W. Terban, S. Canossa, M. Etter, R. E. Dinnebier and B. V. Lotsch, *Adv. Mater.*, 2023, 2210613.

31 J. Lyu, X. Gong, S.-J. Lee, K. Gnanasekaran, X. Zhang, M. C. Wasson, X. Wang, P. Bai, X. Guo, N. C. Gianneschi and O. K. Farha, *J. Am. Chem. Soc.*, 2020, **142**, 4609–4615.

32 H. L. B. Boström, S. Emmerling, F. Heck, C. Koschnick, A. J. Jones, M. J. Cliffe, R. A. Natour, M. Bonneau, V. Guillerm, O. Shekhah, M. Eddaoudi, J. Lopez-Cabrelles, S. Furukawa, M. Romero-Angel, C. Martí-Gastaldo, M. Yan, A. J. Morris, I. Romero-Muñiz, Y. Xiong, A. E. Platero-Prats, J. Roth, W. L. Queen, K. S. Mertin, D. E. Schier, N. R. Champness, H. H. -M. Yeung and B. V. Lotsch, *Adv. Mater.*, 2023, e2304832.

33 P. Gilding, *Nature*, 2019, **573**, 311.

34 P. Gotico, Z. Halime and A. Aukauloo, *Dalton Trans.*, 2020, **49**, 2381–2396.

35 J. Chu, F.-S. Ke, Y. Wang, X. Feng, W. Chen, X. Ai, H. Yang and Y. Cao, *Commun. Chem.*, 2020, **3**, 5.

36 Y. Wang, Q. Li, W. Shi and P. Cheng, *Chin. Chem. Lett.*, 2020, **31**, 1768–1772.

37 M. A. Mushtaq, M. Arif, G. Yasin, M. Tabish, A. Kumar, S. Ibraheem, W. Ye, S. Ajmal, J. Zhao, P. Li, J. Liu, A. Saad, X. Fang, X. Cai, S. Ji and D. Yan, *Renewable Sustainable Energy Rev.*, 2023, **176**, 113197.

38 I. Bhugun, D. Lexa and J.-M. Savéant, *J. Am. Chem. Soc.*, 1996, **118**, 3982–3983.

39 J. Bonin, A. Maurin and M. Robert, *Coord. Chem. Rev.*, 2017, **334**, 184–198.

40 C.-X. Zhao, B.-Q. Li, J.-N. Liu, J.-Q. Huang and Q. Zhang, *Chin. Chem. Lett.*, 2019, **30**, 911–914.

41 T. Wang, Z. Guo, X. Zhang, Q. Li, A. Yu, C. Wu and C. Sun, *J. Mater. Sci. Technol.*, 2023, **140**, 121–134.

42 S.-C. Qi, Z.-H. Yang, R.-R. Zhu, X.-J. Lu, D.-M. Xue, X.-Q. Liu and L.-B. Sun, *J. Mater. Chem. A*, 2021, **9**, 24510–24516.

43 P. M. Stanley, K. Hemmer, M. Hegelmann, A. Schulz, M. Park, M. Elsner, M. Cokoja and J. Warnan, *Chem. Sci.*, 2022, **13**, 12164–12174.

44 M. Zhao, Y. Wang, Q. Ma, Y. Huang, X. Zhang, J. Ping, Z. Zhang, Q. Lu, Y. Yu, H. Xu, Y. Zhao and H. Zhang, *Adv. Mater.*, 2015, **27**, 7372–7378.

45 M. Cong, X. Chen, K. Xia, X. Ding, L. Zhang, Y. Jin, Y. Gao and L. Zhang, *J. Mater. Chem. A*, 2021, **9**, 4673–4678.

46 D. Yao, C. Tang, L. Li, B. Xia, A. Vasileff, H. Jin, Y. Zhang and S. Qiao, *Adv. Energy Mater.*, 2020, **10**, 2001289.

47 Y. Liu, C. Li, L. Guan, K. Li and Y. Lin, *J. Phys. Chem. C*, 2020, **124**, 18003–18009.

48 S. Luo, X. Li, M. Wang, X. Zhang, W. Gao, S. Su, G. Liu and M. Luo, *J. Mater. Chem. A*, 2020, **8**, 5647–5654.

49 L. Wen, X. Li, R. Zhang, H. Liang, Q. Zhang, C. Su and Y.-J. Zeng, *ACS Appl. Mater. Interfaces*, 2021, **13**, 14181–14188.

50 R. Zhang, L. Jiao, W. Yang, G. Wan and H.-L. Jiang, *J. Mater. Chem. A*, 2019, **7**, 26371–26377.

51 (*a*) S. Luo, X. Li, W. Gao, H. Zhang and M. Luo, *Sustainable Energy Fuels*, 2019, **4**, 164–170; (*b*) X. Liang, X. Ren, Q. Yang, L. Gao, M. Gao, Y. Yang, H. Zhu, G. Li, T. Ma and A. Liu, *Nanoscale*, 2021, **13**, 2843–2848; (*c*) X. He, Y. Liao, J. Tan, G. Li and F. Yin, *Electrochim. Acta*, 2022, **409**, 139988.

52 G. Li and F. Yin, *Electrochim. Acta*, 2022, 139988.

This journal is © The Royal Society of Chemistry 2024

J. Mater. Chem. A, 2024, **12**, 10956–10964 | **10963**

53 J. B. Decoste, G. W. Peterson, M. W. Smith, C. A. Stone and C. R. Willis, *J. Am. Chem. Soc.*, 2012, **134**, 1486–1489.

54 T.-H. Chen, I. Popov, O. Zenasni, O. Daugulis and O. Š. Miljanić, *Chem. Commun.*, 2013, **49**, 6846–6848.

55 J. Castells-Gil, F. Novio, N. M. Padial, S. Tatay, D. Ruíz-Molina and C. Martí-Gastaldo, *ACS Appl. Mater. Interfaces*, 2017, **9**, 44641–44648.

56 Y. Lv, Y. Wang, M. Yang, Z. Mu, S. Liu, W. Ding and M. Ding, *J. Mater. Chem. A*, 2020, **9**, 1480–1486.

57 H. He, H.-K. Li, Q.-Q. Zhu, C.-P. Li, Z. Zhang and M. Du, *Appl. Catal., B*, 2022, **316**, 121673.

58 L. Wen, K. Sun, X. Liu, W. Yang, L. Li and H. Jiang, *Adv. Mater.*, 2023, **35**, 2210669.

59 S. Hamad, N. C. Hernandez, A. Aziz, A. R. Ruiz-Salvador, S. Calero and R. Grau-Crespo, *J. Mater. Chem. A*, 2015, **3**, 23458–23465.

60 J. Heyrovský, *Recl. Trav. Chim. Pays-Bas*, 1927, **46**, 582–585.

61 A. R. Kucernak and C. Zalitis, *J. Phys. Chem. C*, 2016, **120**, 10721–10745.

10964 | *J. Mater. Chem. A*, 2024, **12**, 10956–10964

This journal is © The Royal Society of Chemistry 2024